Letters

Magnetic Coupling Visualization Using Sensitivity to Magnetic Permeability

Katsuya Nomura, *Member, IEEE*

***Abstract*—This letter presents a method for visualizing magnetic coupling based on its sensitivity to magnetic permeability. Because a magnetic flux causes magnetic coupling that is proportional to permeability, an increase in permeability along the propagation path strengthens the magnetic coupling, whereas an increase in permeability outside the path has little effect on the coupling. The propagation path for magnetic coupling can thus be visualized based on the sensitivity to permeability. Calculating this sensitivity is faster than performing an electromagnetic simulation using the adjoint variable method. Two examples, namely, a loop pair and a simple electromagnetic interference filter, are used to show that the propagation path due to magnetic coupling can be visualized using the proposed method.**

***Index Terms*—Adjoint variable method, magnetic coupling, sensitivity, visualization.**

I. Introduction

THE identification of dominant parasitic coupling is important for electromagnetic compatibility (EMC) design [1], [2]. In magnetic field coupling [3], which is a major type of coupling, the magnetic flux from a magnetic field source flows along a propagation path to the receiving point and generates an induced current by penetrating the parasitic receiving loop. Unlike conducted noise, noise due to magnetic coupling is not transmitted along conductors, making it difficult to optimize the design of a system in terms of EMC.

An electromagnetic interference (EMI) scanning system [4], [5] or an electromagnetic field analysis [6] is commonly used to identify the locations of strong magnetic fields. However, a strong magnetic field is not always the source of the radiation that causes EMC problems. In addition, these methods cannot identify the propagation path and the receiving point.

Methods for identifying and visualizing coupling paths using energy parcels [7], [8] or impedance density [9], [10], [11] have been developed. Although these methods can directly visualize energy propagation or mutual coupling, they use a physical quantity defined by the product of the electric field and the magnetic field, making it difficult to distinguish between magnetic field coupling and electric field coupling. Different noise reduction methods are suitable for different coupling mechanisms; a shield with two terminations effectively reduces inductive coupling and a shield with one termination effectively reduces capacitive coupling [12]. Thus, it is important for EMC design to distinguish magnetic field coupling from electric field coupling.

This letter presents a method for visualizing magnetic coupling based on the sensitivity to magnetic permeability. The rest of this letter is organized as follows. The principle of the visualization method and a fast sensitivity analysis method are explained in Section II. Two examples used for verifying the proposed method are given in Section III. Finally, Section IV concludes this article.

II. Method

Noise propagation characteristics are evaluated using the S-parameter S_{21}, whose value depends on various factors, including magnetic field coupling. If magnetic field coupling is dominant, the magnet flux, which is proportional to permeability, along the propagation path greatly affects S_{21}; an increase in permeability along the propagation path strengthens the coupling and increases $|S_{21}|$, whereas an increase in permeability outside the path has little effect on $|S_{21}|$. Therefore, magnetic field coupling can be visualized using the partial derivative of $|S_{21}|$ to magnetic permeability, which is called the sensitivity.

The sensitivity can be written as

$$\frac{\partial |S_{21}|}{\partial \mu_{r\_i}} \tag{1}$$

where μ_{r_i} is the relative permeability of the ith element. This expression implies that the sensitivity can be obtained numerically and that the analysis domain can be divided into many elements by discretization. The finite element method (FEM) is used here as the numerical method. When calculating the sensitivity using the difference method, the number of required forward analyses almost equals the number of elements. In contrast, when calculating the sensitivity using the adjoint variable method, only one forward analysis is required. In the adjoint variable method, the extended objective function J^* is defined as

$$J^* = J + \boldsymbol{\lambda}^{\mathrm{T}} (\mathrm{K}\boldsymbol{e} - \boldsymbol{f}) \tag{2}$$

where J is the objective function, which corresponds to $|S_{21}|$ in this case, K is the stiffness matrix derived from the FEM, $\boldsymbol{e}$ is the electric field vector, $\boldsymbol{f}$ is the nodal force vector, and $\boldsymbol{\lambda}$ is the

Manuscript received 14 September 2023; revised 17 November 2023; accepted 16 December 2023. This work was supported by the Japan Society for the Promotion of Science KAKENHI under Grant 22K14248.

The author is with the School of Engineering, Kwansei Gakuin University, Sanda 669-1330, Japan (e-mail: katsuya.nomura@kwansei.ac.jp).

Color versions of one or more figures in this article are available at https://doi.org/10.1109/TEMC.2023.3344887.

Digital Object Identifier 10.1109/TEMC.2023.3344887

adjoint variable vector. The sensitivity can be written as

$$\begin{aligned}\frac{\partial J}{\partial \mu_{r\_i}} &= \frac{\partial J^*}{\partial \mu_{r\_i}} = \frac{\partial J}{\partial \boldsymbol{e}}\frac{\partial \boldsymbol{e}}{\partial \mu_{r\_i}} + \boldsymbol{\lambda}^{\mathrm{T}}\left(\frac{\partial \mathrm{K}}{\partial \mu_{r\_i}}\boldsymbol{e} + \mathrm{K}\frac{\partial \boldsymbol{e}}{\partial \mu_{r\_i}} - \frac{\partial \boldsymbol{f}}{\partial \mu_{r\_i}}\right) \\ &= \left(\frac{\partial J}{\partial \boldsymbol{e}} + \boldsymbol{\lambda}^{\mathrm{T}}\mathrm{K}\right)\frac{\partial \boldsymbol{e}}{\partial \mu_{r\_i}} + \boldsymbol{\lambda}^{\mathrm{T}}\left(\frac{\partial \mathrm{K}}{\partial \mu_{r\_i}}\boldsymbol{e} - \frac{\partial \boldsymbol{f}}{\partial \mu_{r\_i}}\right). \end{aligned} \tag{3}$$

By solving the adjoint equation

$$\left(\frac{\partial J}{\partial \boldsymbol{e}} + \boldsymbol{\lambda}^{\mathrm{T}}\mathrm{K}\right) = \boldsymbol{0} \tag{4}$$

the calculation of $\partial \boldsymbol{e}/\partial \mu_{r\_i}$ can be omitted and the sensitivity can be evaluated using only the second term, which greatly reduces the computational cost.

Sensitivity analysis using the adjoint variable method is a very well known technique in topology optimization [13], which is a structural optimization method that iteratively updates the structure based on sensitivity information. Topology optimization, originally developed for structural design, has been applied to electromagnetic design problems and optimization using the FEM [14], the finite-difference time-domain (FDTD) method [15], and the method of moments [16]. Although the sensitivity can be obtained using these three methods, only the FEM and the FDTD method are suitable for magnetic path visualization in the proposed method because sensitivity information regarding the air domain around the target structure is important.

In practice, the value of sensitivity in (1) depends on the volume of the element; a larger element leads to a larger value. Therefore, the following normalized sensitivity is evaluated for visualization:

$$\frac{1}{V_i}\frac{\partial |S_{21}|}{\partial \mu_{r\_i}} \tag{5}$$

where V_i is the volume of the ith element.

III. Numerical Examples

The proposed method is verified using two examples, namely a loop pair and an EMI filter. The loop pair is an example of pure magnetic field coupling, while the EMI filter is an example of inductive noise and conductive noise mixed together. COMSOL multiphysics and its RF and optimization modules were used for the electromagnetic and sensitivity analyses. All computation was conducted by COMSOL by following three steps.

1) Discretize the weak form of the wave equation derived from Maxwell's equations, and solve the matrix equation, that is, $\mathrm{K}\boldsymbol{e} = \boldsymbol{f}$. This step determines the electric field vector $\boldsymbol{e}$.
2) Solve the adjoint (4). This step determines the adjoint variable vector $\boldsymbol{\lambda}$.
3) Calculate the sensitivity $\frac{\partial J}{\partial \mu_{r\_i}}$ as $\boldsymbol{\lambda}^{\mathrm{T}}\left(\frac{\partial \mathrm{K}}{\partial \mu_{r\_i}}\boldsymbol{e} - \frac{\partial \boldsymbol{f}}{\partial \mu_{r\_i}}\right)$. This step determines the normalized sensitivity $\frac{1}{V_i}\frac{\partial |S_{21}|}{\partial \mu_{r\_i}}$.

The sensitivity calculation was conducted using symbolic partial differentiation and the chain rule as stated in the COMSOL user's guide [17].

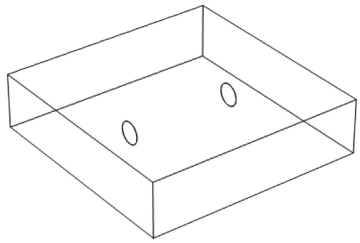

Fig. 1. Diagram of loop pair structure.

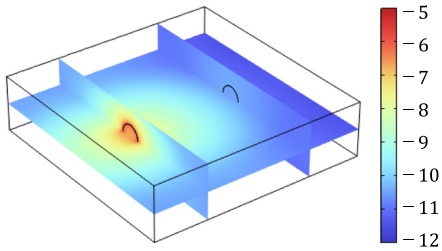

Fig. 2. Log of magnetic flux density amplitude, $\log_{10}(|\boldsymbol{B}|)$, for loop pair.

A. Loop Pair

The loop pair structure is shown in Fig. 1. In an air box with dimensions of 2000, 2000, and 500 mm, two torus-shaped metal loops with a major radius of 100 mm and a minor radius of 1 mm are set with a separation distance of 1000 mm. Ports 1 and 2 are set as the left and right loops, respectively. The left loop is excited at 10 MHz and the normalized sensitivity in (5) is calculated. At this frequency, the wavelength is almost 30 m and the loops are thus regarded as small loop antennas.

Electromagnetic and sensitivity analyses were conducted on a computer with a dual-core CPU (Xeon 4214R) and 256 GB of RAM. The computational times were 16 and 10 s, respectively. As shown in Fig. 2, although the flux density amplitude is high only around the left loop, which is the magnetic source, the normalized sensitivity is high around both loops and between the loops, as shown in Fig. 3. This confirms that propagation due to magnetic coupling can be visualized using the sensitivity.

B. EMI Filter

The proposed method is applied to a simple EMI filter. The circuit diagram and structure of the filter are shown in Figs. 4 and 5, respectively. In this *C-L-C-L-C* filter circuit, the dominant noise depends on the circuit parameters [18]. When the inductances of L1 and L2 are small, the conduction noise directly flows from port 1 to port 2 via L1 and L2; magnetic coupling is negligible in this case. On the other hand, when the inductances of L1 and L2 are sufficiently large, the conduction noise is suppressed and instead the induction current due to magnetic coupling between the input and output loops becomes dominant. Fig. 6(a) and (b) shows the noise propagation path for these two cases, respectively.

The situations corresponding to these two cases were realized by a simulation at 10 MHz with the circuit parameters given in Table I. First, to confirm that the dominant paths are different

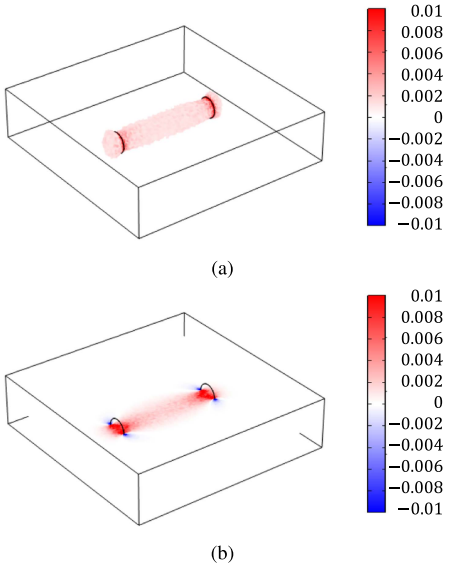

Fig. 3. Normalized sensitivity (a) in analytic domain and (b) on plane. In (a), only domains with values greater than 0.001 are plotted.

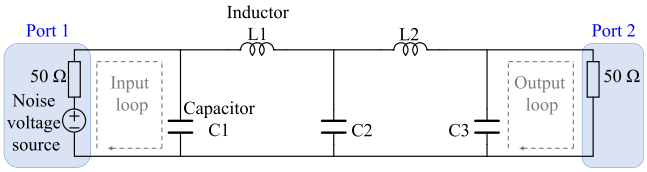

Fig. 4. Circuit diagram for simple EMI filter.

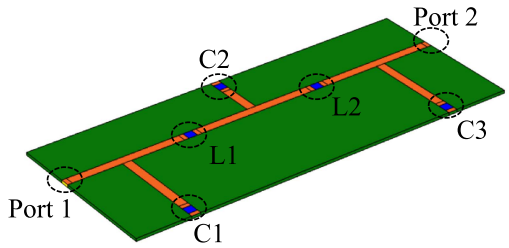

Fig. 5. Structure of simple EMI filter.

TABLE I
CIRCUIT PARAMETERS FOR SIMPLE EMI FILTER

Setting	C1, C2, C3	L1, L2
1	20 μF	0.1 μH
2	20 nF	1 mH

in the two settings, the effect of doubling the values of L1 and L2 on $|S_{21}|$ was examined. The results are given in Table II. It was found that setting 1 took a conductive path because $|S_{21}|$ decreased as inductance increased, while setting 2 took an inductive path because inductance had no effect on $|S_{21}|$.

A sensitivity analysis was conducted at 10 MHz under the two parameter settings given in Table I. For both settings, the computational times for the electromagnetic and sensitivity analyses were 37 and 21 s, respectively, on the same computer used in the loop pair example.

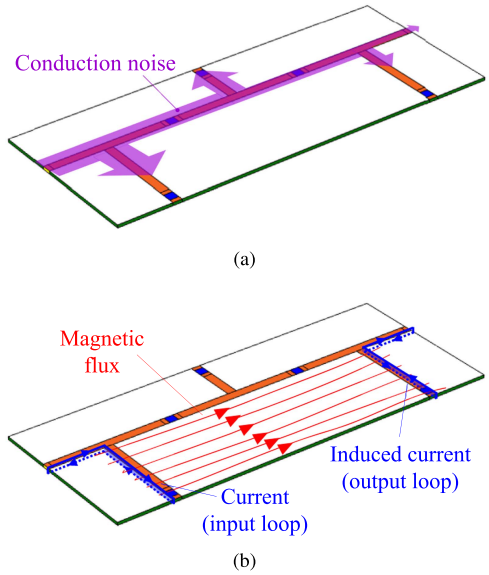

Fig. 6. Noise propagation paths in simple EMI filter. (a) Conductive path and (b) inductive path.

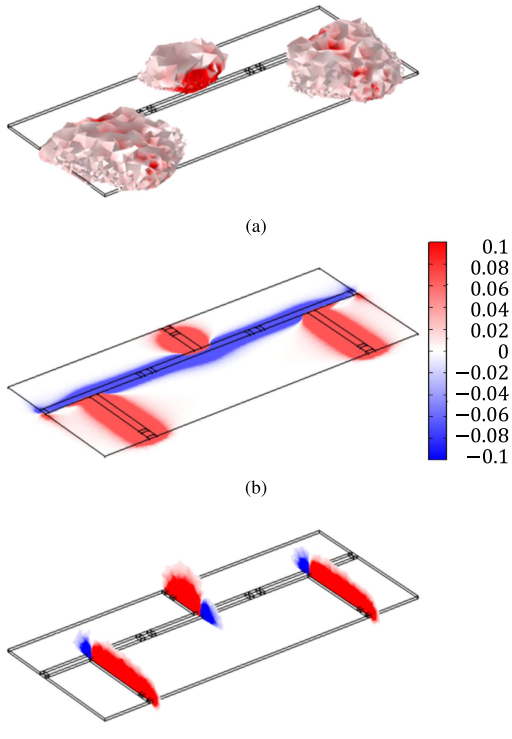

Fig. 7. Normalized sensitivity (a) in analytic domain, (b) on *x*-*y* plane, and (c) on *y*-*z* plane for setting 1. In (a) and (c), only values and absolute values greater than 0.001 are plotted, respectively.

TABLE II
$|S_{21}|$ VALUES UNDER ORIGINAL AND DOUBLED INDUCTANCES

Setting	Original L1 and L2 values	Doubled L1 and L2 values	Dominant path
1	-81.64 dB	-91.24 dB	Conductive path
2	-116.56 dB	-116.56 dB	Inductive path

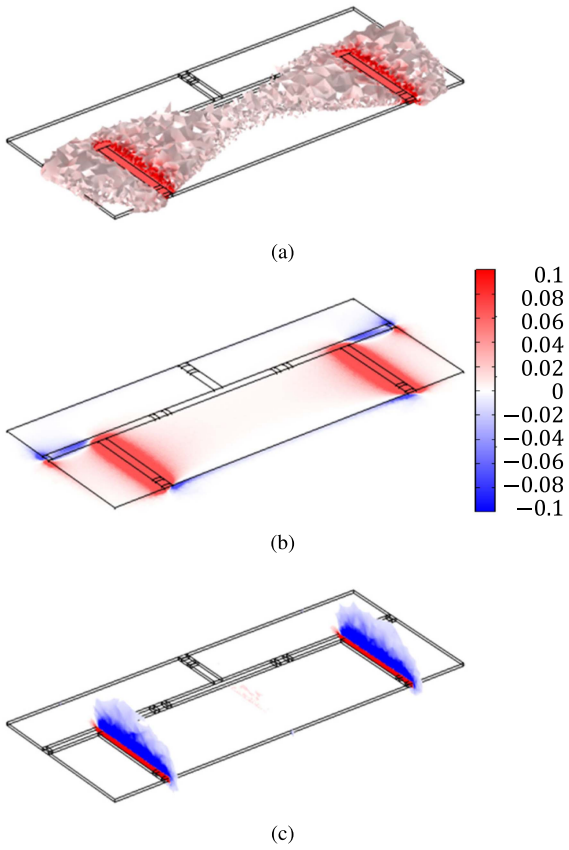

Fig. 8. Normalized sensitivity (a) in analytic domain, (b) on x-y plane, and (c) on y-z plane for setting 2. In (a) and (c), only values and absolute values greater than 0.001 are plotted, respectively.

Figs. 7 and 8 show the sensitivity for settings 1 and 2, respectively. As shown in Fig. 7(a) and (b), when conductive noise is dominant, the sensitivity is greater above the conductors connected to the capacitors. This implies that increasing the permeability in this region increases the parasitic inductance, which degrades the bypass performance and increases $|S_{21}|$. On the other hand, as shown in Fig. 8(a) and (b), when inductive noise is dominant, a region with high sensitivity appears between the input and output loops; the magnetic coupling can thus be visualized. Figs. 7(c) and 8(c) support these arguments. In Fig. 7(c), the sensitivity is high above the three patterns connected to the capacitor. In Fig. 8(c), the sensitivity is high inside the input and output loops but low outside the loops; this indicates that higher permeability inside the loops strengthens the magnetic field coupling, whereas higher permeability outside the loops causes the magnetic flux to deviate from the loop. A negative sensitivity means that S_{21} decreases as permeability increases, as can be explained from the sensitivity definition.

Thus, the sensitivity distribution strongly depends on the noise propagation path, which can help identify the magnetic coupling.

IV. Conclusion and Future Work

In this letter, a method for visualizing magnetic coupling was proposed and verified. The method uses the sensitivity distribution of $|S_{21}|$ with respect to magnetic permeability to evaluate the effect of magnetic flux on the transmission characteristics. Two simple examples, namely, a loop pair and a *C-L-C-L-C* EMI filter, confirmed the effectiveness of the proposed method. In the future, this method will be applied to more realistic structures. It may be possible to visualize the electric field coupling by using the sensitivity of the dielectric permittivity. This is a topic for future work. Reflecting the results of the visualization for product design is also a subject for future work.

References

[1] C. R. Paul, "The concept of dominant effect in EMC," *IEEE Trans. Electromagn. Compat.*, vol. 34, no. 3, pp. 363–367, Aug. 1992.
[2] C. R. Paul, *Introduction to Electromagnetic Compatibility*. Hoboken, NJ, USA: Wiley, 2006.
[3] R. Wang, H. F. Blanchette, M. Mu, D. Boroyevich, and P. Mattavelli, "Influence of high-frequency near-field coupling between magnetic components on EMI filter design," *IEEE Trans. Power Electron.*, vol. 28, no. 10, pp. 4568–4579, Oct. 2013.
[4] H. He, P. Maheshwari, and D. J. Pommerenke, "The development of an EM-field probing system for manual near-field scanning," *IEEE Trans. Electromagn. Compat.*, vol. 58, no. 2, pp. 356–363, Apr. 2016.
[5] T. Ibuchi and T. Funaki, "Visualization of dynamic noise current distribution from Si and SiC power devices based on time-synchronized near magnetic field scanning," in *Proc. Int. Symp. Electromagn. Compat.*, 2020, pp. 1–6.
[6] B. Zhang and S. Wang, "Analysis and reduction of the near magnetic field emission from toroidal inductors," *IEEE Trans. Power Electron.*, vol. 35, no. 6, pp. 6251–6268, Jun. 2020.
[7] H. Li, V. V. Khilkevich, and D. Pommerenke, "Identification and visualization of coupling paths–Part I: Energy parcel and its trajectory," *IEEE Trans. Electromagn. Compat.*, vol. 56, no. 3, pp. 622–629, Jun. 2014.
[8] H. Li, V. V. Khilkevich, and D. Pommerenke, "Identification and visualization of coupling paths–Part II: Practical application," *IEEE Trans. Electromagn. Compat.*, vol. 56, no. 3, pp. 630–637, Jun. 2014.
[9] J. Malmström, H. Holter, and B. L. G. Jonsson, "On mutual coupling and coupling paths between antennas using the reaction theorem," *IEEE Trans. Electromagn. Compat.*, vol. 60, no. 6, pp. 2037–2040, Dec. 2018.
[10] J. Lundgren, J. Malmström, J.-M. Hannula, and B. L. G. Jonsson, "Visualization and reduction of mutual coupling between antennas installed on a platform," *IEEE Trans. Electromagn. Compat.*, vol. 64, no. 1, pp. 92–101, Feb. 2022.
[11] Y. Zhong, W. Song, C. Kim, and C. Hwang, "Coupling path visualization and its application in preventing electromagnetic interference," *IEEE Trans. Electromagn. Compat.*, vol. 62, no. 4, pp. 1485–1492, Aug. 2020.
[12] H. W. Ott, *Electromagnetic Compatibility Engineering*. Hoboken, NJ, USA: Wiley, 2011.
[13] M. P. Bendsøe and O. Sigmund, *Topology Optimization: Theory, Methods, and Applications*. Berlin, Germany: Springer-Verlag2004.
[14] K. Nomura et al., "Topology optimization of conductors in electrical circuit," *Struct. Multidisciplinary Optim.*, vol. 59, no. 6, pp. 2205–2225, 2019.
[15] T. Nomura, K. Sato, K. Taguchi, T. Kashiwa, and S. Nishiwaki, "Structural topology optimization for the design of broadband dielectric resonator antennas using the finite difference time domain technique," *Int. J. Numer. Methods Eng.*, vol. 71, no. 11, pp. 1261–1296, 2007.
[16] S. Zhou, W. Li, and Q. Li, "Level-set based topology optimization for electromagnetic dipole antenna design," *J. Comput. Phys.*, vol. 229, no. 19, pp. 6915–6930, 2010.
[17] COMSOL, "Optimization module user's guide," version 5.4, 2018.
[18] K. Nomura et al., "Topology-optimization-Based EMC design," in *Proc. Int. Symp. Electromagn. Compat.*, 2019, pp. 933–937.